Imaging biliary lipid secretion in the rat: ultrastructural evidence for vesiculation of the hepatocyte canalicular membrane[1]

James M. Crawford,[2,*] Gotthold-Mathias Möckel,† Aleta R. Crawford,* Susan J. Hagen,† Victoria C. Hatch,§ Stephen Barnes, John J. Godleski,*,§ and Martin C. Carey†**

Departments of Pathology* and Medicine, Division of Gastroenterology,† Brigham and Women's Hospital, Harvard Medical School, and Harvard Digestive Diseases Center, Boston, MA 02115; Division of Respiratory Biology,§ Harvard School of Public Health, Boston, MA 02115; and Department of Pharmacology,** University of Alabama at Birmingham, Birmingham, AL 35294

Abstract Physical-chemical and biological studies of hepatic bile suggest that biliary phospholipid molecules are secreted as unilamellar vesicles. Systematic ultrastructural studies of bile canaliculi were undertaken to visualize this event. Liver tissue was obtained from normal adult male rats (control), from bile salt-depleted rats (by overnight biliary diversion), and from depleted rats infused intravenously with a hydrophilic-hydrophobic congener series of common taurine-conjugated bile salts. Livers were fixed in situ either by modified chemical methods or by ultrarapid cryofixation. In control rats, chemical fixation revealed unilamellar vesicles 63 ± 17 (± SD) nm in diameter, mostly free within canalicular lumena. Vesicles were infrequent in canaliculi of bile salt-depleted rats, but were present in canaliculi of rats infused with taurocholate. In cryofixed liver tissue, vesicles 67 ± 13 nm in diameter were observed in canaliculi of control rats and bile-salt depleted rats infused with common bile salts. The majority of these vesicles were affixed to the luminal side of the canalicular membrane. The average number of vesicles per bile canaliculus was in agreement with that estimated on the basis of biliary phospholipid secretion rates, mean vesicle size, and area of close-packed phosphatidylcholine molecules. By immunoelectron microscopy, canalicular vesicles were free of actin and of a 100 kDa canalicular membrane protein. We conclude that biliary phospholipid molecules are secreted from hepatocytes into bile canalicular lumena as unilamellar vesicles ~63–67 nm in average diameter. We postulate that this secretion mechanism involves lumenal bile salt-induced vesiculation of lipid microdomains in the exoplasmic hemileaflet of the canalicular membrane.—**Crawford, J. M., G-M. Möckel, A. R. Crawford, S. J. Hagen, V. C. Hatch, S. Barnes, J. J. Godleski, and M. C. Carey.** Imaging biliary lipid secretion in the rat: ultrastructural evidence for vesiculation of the hepatocyte canalicular membrane. *J. Lipid Res.* 1995. **36:** 2147–2163.

Supplementary key words liver • bile salt • vesicle • bile canaliculus • electron microscopy • cryofixation

Bile is the lipid-rich hepatic secretion that is necessary for elimination of cholesterol and xenobiotics from the body, and for dispersion and efficient absorption of digested dietary lipid in the upper small intestine. Bile salts and phospholipids (primarily phosphatidylcholine) are the main organic solutes in bile, and play a crucial role in cholesterol and dietary lipid solubilization. Although progress has been made in understanding hepatocellular bile salt secretion (1), the processes by which bile salts induce phospholipid secretion have not been identified. A particular challenge has been to understand how biliary phosphatidylcholine molecules are

Abbreviations: CMC, critical micelle concentration; HPLC, high performance liquid chromatography; PBS, phosphate-buffered saline; PC-TP, phosphatidylcholine-transfer protein; PIPES, 1,4-piperazine diethane sulfonic acid; TEM, transmission electron microscopy; TDHC, taurodehydrocholate ([3,7,12-trioxo-5β-cholan-24-oyl]-2-aminoethanesulfonic acid); TUC, tauroursocholate([3α,7β,12α-trihydroxy-5β-cholan-24-oyl]-2-aminoethane-sulfonic acid); TMC, tauromuricholate (1:1 mixture of [3α,6β,7α- and 3α,6β,7β-trihydroxy-5β-cholan-24-oyl]-2-aminoethanesulfonic acids); TUDC, tauroursodeoxycholate ([3α,7β-dihydroxy-5β-cholan-24-oyl]-2-aminoethanesulfonic acid); TC, taurocholate ([3α,7α,12α-trihydroxy-5β-cholan-24-oyl]-2-aminoethanesulfonic acid); TCDC, taurocheno-deoxycholate ([3α,7α-dihydroxy-5β-cholan-24-oyl]-2-aminoethane-sulfonic acid).

[1]Dedicated to the memory of Dr. Möckel, a brilliant and beloved colleague who began these studies during a post-doctoral fellowship from 1986 to 1988.

[2]To whom correspondence should be addressed at: Department of Pathology, Brigham and Women's Hospital, 75 Francis Street, Boston, MA 02115.

secreted continuously and in large quantities without incurring disruption of the canalicular membrane.

Biliary-specific phosphatidylcholine molecules are recruited initially from intracellular sources, predominantly the endoplasmic reticulum (2). A proposed mechanism for phosphatidylcholine delivery to the canalicular plasma membrane is monomeric transfer via binding to cytosolic phosphatidylcholine transfer protein (PC-TP; (3)), a process which is stimulated by low concentrations of bile salts typical of the hepatocyte's cytosol. Alternatively, biliary lipid may arrive at the canalicular membrane via intracellular vesicle transport (4). Once delivered to the canalicular membrane, it is postulated (5, 6) that biliary phosphatidylcholine molecules are translocated from the endoplasmic to the exoplasmic hemileaflet by the action of a transmembrane translocator (7), a function that appears to be absent in the mouse deficient for the mdr2 (multiple drug resistance 2) P-glycoprotein gene product (8). The next step in bile salt-induced phosphatidylcholine secretion is unknown. Both exovesiculation of microdomains of biliary lipid and selective extraction of biliary lipid from the canalicular membrane have been proposed (6, 9, 10). The secretion process is dependent upon the presence of an appreciable concentration of luminal bile salts (11), which are thought (12–16) to generate lipid vesicles, as seen occasionally in electron micrographs of bile canaliculi (e.g., (14, 15, 17–19)). Lipid vesicles approximately 60 to 80 nm in diameter have been documented repeatedly by electron microscopy and quasielastic light scattering of freshly secreted hepatic biles (12–14, 20–22). Microscope laser light scattering of bile canaliculi in isolated rat hepatocyte couplets also detects intraluminal vesicles of similar size, the numbers of which increase upon cellular incubation with bile salts (23). Thus, this study was undertaken to systematically evaluate the hypothesis that the principal means of hepatocyte phospholipid secretion is elaboration of vesicles by the canalicular membrane.

MATERIALS AND METHODS

Chemical reagents

The sodium salts of taurodehydrocholate (TDHC), tauroursocholate (TUC), tauroursodeoxycholate (TUDC), taurocholate (TC), and taurochenodeoxycholate (TCDC) were purchased from Calbiochem, La Jolla, CA. The purity of all commercial bile salts exceeded 99% by high-performance liquid chromatography (HPLC, (24)). Tauromuricholate (TMC) was the kind gift from Drs. Ashok Batta and Gerald Salen (Newark, NJ), and was an approximately equimolar mixture of 3α,6β,7α- and 3α,6β,7β-hydroxyl isomers, as measured by immobilized artificial membrane HPLC (25). 3α-Hydroxysteroid dehydrogenase for the bile salt assay was obtained from Worthington Diagnostic Systems, Inc., Freehold, NJ. Osmium tetroxide crystals were obtained from Stevens Metallurgical Co., New York, NY. IgG raised in rabbits to chicken gizzard actin and preimmune rabbit IgG were obtained from Biomedical Technologies, Inc. (Stoughton, MA). Rabbit antiserum to the canalicular 100 kDa ectoATPase bile salt transporter (26) and preimmune rabbit serum were kind gifts from Drs. M. Ananthanarayanan and F. J. Suchy (New Haven, CT). Biotin-labeled goat anti-rabbit IgG was from Gibco Research Products (Gaithersburg, MD), and Auroprobe EM Streptavidin G10 (10 nm gold-streptavidin) was from Amersham Life Science (Arlington Heights, IL). All other reagents were of the highest grades commercially available.

Animal preparation

Adult male Sprague-Dawley rats (231 ± 24 g, ± SD, n = 43 for chemical fixation studies; 268 ± 7 gm, n = 8 for cryofixation studies) were maintained on a 12-h light/12-h dark cycle and given Purina rat chow and water ad libitum prior to study. An 18-day-old male Sprague-Dawley suckling rat (32 g) also was utilized in the cryofixation studies because of the immaturity of its biliary lipid secretory function and hence decreased rates of phospholipid secretion (27).

Control animals and the suckling animal were anesthetized and the liver was fixed in situ (see below). Other adult animals were fitted with intravenous and biliary catheters (PE-10 polyethylene tubing, Clay Adams Division, Beckton, Dickinson and Co., Parsippany, NJ) under light ether anesthesia the day prior to killing (28). Animals were placed in restraining cages, maintained at 37°C under heating lamps, hydrated via an intravenous infusion of 0.15 M NaCl at 1.5 ml/h, and allowed access to water (chemical fixation studies), or water and rat chow (cryofixation studies) ad libitum. After overnight biliary diversion, animals received a 1-h i.v. bile salt infusion in albumin-free 0.15 M NaCl at 1.5 ml/h. Previous work has shown that bile flow and secretion rates for bile salts, phospholipid, and cholesterol reach steady state after 30 min of bile salt infusion (28), and that hemolysis is not encountered at these doses, with the exception of i.v. TCDC where minimal hemolysis occurs (29). Bile was collected continuously, and the final 15-min samples were analyzed for biliary lipids. For in situ liver fixation, each animal was then anesthetized with ether (chemical fixation studies) or sodium pentobarbital (cryofixation studies, 50 mg/kg i.p.). Rectal temperature was maintained at 37.0 ± 0.5°C by means of a warming lamp.

Chemical fixation of liver tissue

To optimize morphologic preservation of bile canaliculi and their putative contents, a wide variety of chemical fixation protocols were tested (30–32). The optimal fixation protocol was found to be total body perfusion in situ via the left ventricle, followed by immediate post-fixation in an aldehyde/osmium-containing fixative (33). Specifically, animals were given i.v. heparin (1700 units in 0.3 ml saline), followed by left ventricular perfusion with oxygenated 37°C Hanks' balanced salt solution containing 500 units/ml heparin (Sigma, St. Louis, MO; 30 ml/min for 3 min) and freshly made Fixation Buffer A (half-strength Karnovsky's solution: 2% paraformaldehyde, 2.5% glutaraldehyde, 0.1 M sodium cacodylate, pH 7.4, 37°C; 30 ml/min for 5 min). Liver tissue blocks (0.5 cm^3) were post-fixed by immersion in Fixation Buffer B (Fixation Buffer A freshly mixed 1:1, v:v, with aqueous 2% OsO_4; 10 min × 4 on ice; (34)). Specimens were washed with distilled water and incubated overnight in 2.0% aqueous uranyl acetate at 4°C. After dehydration through graded ethanols and propylene oxide and embedding with LX112 (LADD Research Industries, Inc., Burlington, VT), sections were examined with a Philips 300 electron microscope.

As judged by adequacy of infiltration, preservation of cellular and canalicular ultrastructural features, and visualization of lipid structures within bile canaliculi, fixation of the liver compared favorably with, or was better than, liver tissue fixed by *1)* exposure to OsO_4 prior to glutaraldehyde (35); *2)* substituting phosphate-buffered saline (PBS), bicarbonate, or PIPES for cacodylate in Fixation Buffers A or B; *3)* utilizing full-strength Karnovsky's solution; *4)* addition of $CaCl_2$ or sucrose; *5)* inclusion of 2.5% potassium ferrocyanate in Fixation Buffer B (30); *6)* substituting portal vein for aortic perfusion (17); *7)* omitting corporeal perfusion (36); or *8)* utilizing sodium pentobarbital rather than ether anesthesia at the time of liver harvesting.

Cryofixation and processing of liver tissue

For cryofixation studies, four liver tissue samples without prior heparinization were obtained from each of nine animals. For each sample, a single intact liver lobe was lifted above the abdominal cavity and a tangential razor slice was made into the ventral surface. Ultrarapid cryofixation was performed using the DDK PS1000™ device (Delaware Diamond Knives, Inc., Newark, DE). This hand-held "gun" uses a piston to push tissue against a liquid nitrogen-cooled 3 mm diameter metal mirror enabling vitrification to a tissue depth of about 30 μm. Time between first manipulation of a liver lobe and cryofixation was 2 to 3 sec, and total time for four lobes was < 1.5 min. Two specimens from each rat were freeze-dried using the LifeCell® MDD-C Molecular Distillation Dryer, as previously described (37). Specimens were then exposed at 25°C to fixatives at 10^3 mbar; optimal specimen stabilization was obtained using dry vaporized paraformaldehyde followed by vaporized OsO_4. Specimens were infiltrated with de-gassed Araldite 502 resin and polymerized at 45°C over 2 days.

Electron microscopy of cryofixed specimens

Thin sections (50 nm) were examined, without post-staining, in a Zeiss CEM902 electron microscope (37). Electron spectroscopic imaging provided high image contrast of these lightly stained specimens by obtaining images of the inelastically scattered electrons (38).[3] Each tissue block was cut to obtain four grids containing at least four thin sections. Each grid section was scanned at 250 and 3000 × magnification to identify the cryofixation contact face and the intact cell layers of optimal tissue preservation (39). All bile canaliculi, defined as luminal structures between two or three hepatocytes delimited by intact plasma membranes and tight junctional zones, were identified at 7,000 × magnification, viewed at 30,000 × magnification, and digitized images were obtained.

Morphometric analysis

Digitized images were measured by one individual (ARC) without knowledge of the treatment group. Bile canalicular area was measured using a polygon extending across the base of abutting intracanalicular structures. If not free within the lumen, each intracanalicular structure was defined by the outer circumference of its limiting membrane and its canalicular base. Each structure was identified using a threshold function, and the measured area included the interior. Linear dimensions were measured independently, using line segments and including the thickness of delimiting membranes. Accuracy was evaluated independently by a second individual (JMC) without knowledge of image results obtained by ARC. There was 98% agreement on identification of canalicular vesicles (333 out of 341, see Results). Linear dimensions were reproducible to within 3% (2 nm). Ellipsoid vesicle area calculated from the linear dimensions matched the area measured by threshold analysis to within 5% (equivalent to a variance in axial dimensions of 2 nm). As pixel size at 30,000 × magnification was equivalent to 2.5 nm (data not shown), these findings demonstrated that the average variance of inde-

[3] In this study, electrons decelerated through a 20 eV window were imaged; the range used (240–260 eV) captured electrons that were inelastically scattered by common organic elements.

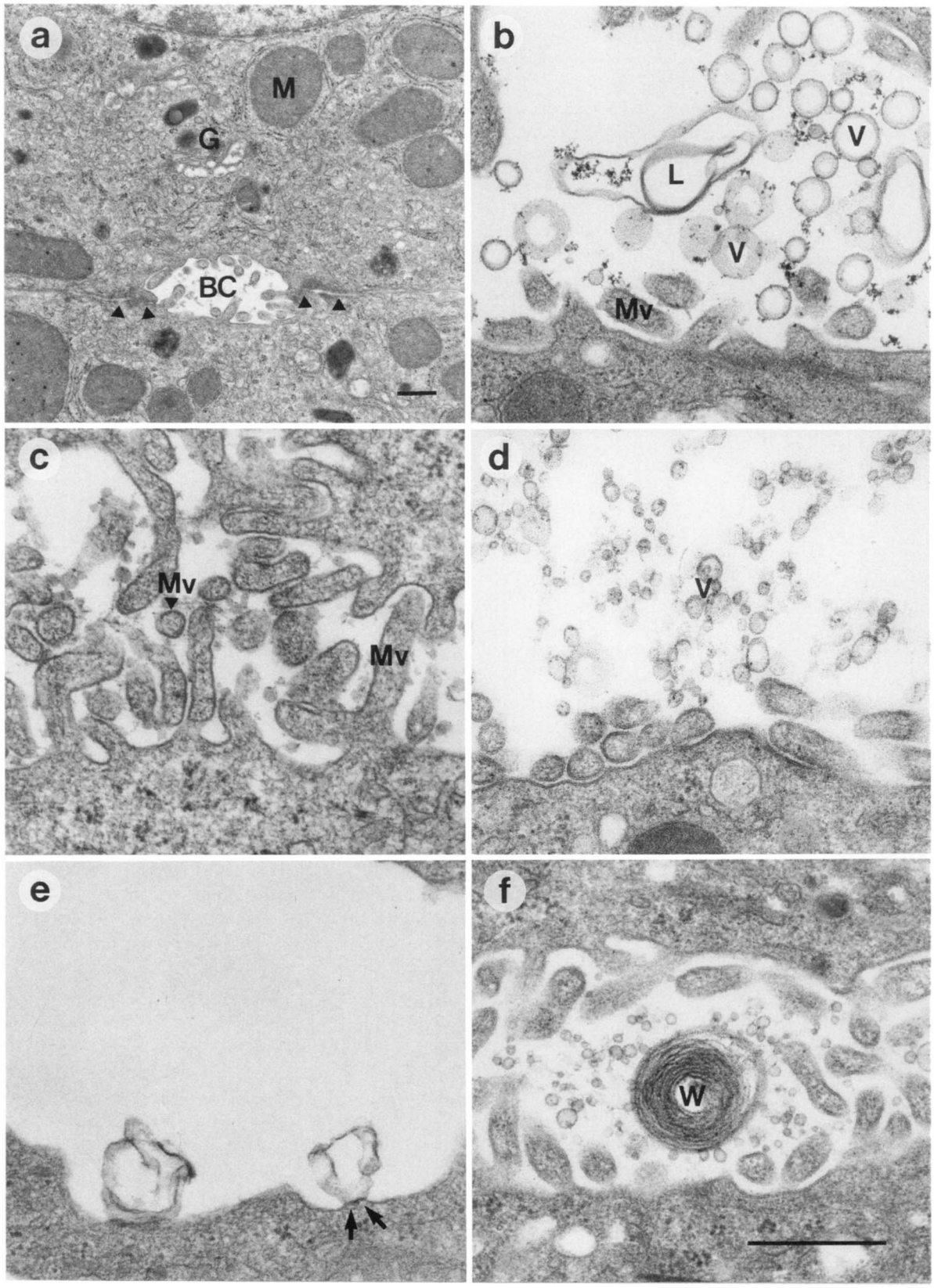

Fig. 1. Electron microscopy of chemically fixed liver tissue. Rat livers were chemically fixed (see Methods) and examined by conventional transmission electron microscopy. (a) Pericanalicular region of two adjoining periportal hepatocytes from control rat (without interruption of the enterohepatic circulation). Labeled structures are the bile canaliculus (BC), mitochondria (M), Golgi apparatus (G), and tight junctional regions (arrowheads), (b) bile canaliculus in control rat, containing unilamellar vesicles (V) within the canalicular lumen and occasionally larger structures (L). Vesicles exhibit electron-lucent interiors, in contrast to microvilli (Mv). (c) Bile canaliculus from bile salt-depleted rat (by overnight biliary diversion). No vesicles are present, and the canaliculus is collapsed. Multiple microvilli (Mv) are present, cut in longitudinal and oblique section. (d) Bile canaliculus from bile salt-depleted rat infused for 1 h with TC at 400 nmol/min per 100 g. When compared to control rat (panel b), vesicles (V) are smaller. (e) Bile canaliculus from control rat, showing two irregular membranous structures with an attachment zone to the bile canalicular membrane (arrows). (f) Bile canaliculus from control rat showing an intracanalicular multilamellar vesicle (membranous whorl, W). (a) Bar = 500 nm; (b, c, d, f) bar = 500 nm; (e) is shown at twofold magnification relative to (f).

pendent measurements by two individuals was equivalent to one pixel in any one direction. Such variance had a negligible effect on results.

Immunoelectron microscopy

Two cryofixed tissue specimens from the TUC-infused rat were processed for electron microscopy as above, but with infiltration and embedding in water-permeable Spurr resin (40). Immunolabeling was performed as described (41) with minor modifications. To remove excess osmium, 50-nm sections were treated first with saturated sodium metaperiodate (42). Sections were then exposed to primary rabbit antibodies (anti-actin IgG diluted 1:10, anti-ectoATPase serum diluted 1:100), biotinylated goat anti-rabbit IgG, and streptavidin/10 nm gold. As controls for the primary incubation step, sections were incubated with buffer or with rabbit preimmune serum (as control for ectoATPase) or rabbit IgG fraction (as control for actin); negligible gold deposition occurred under these conditions. Sections were post-fixed with 1% glutaraldehyde in PBS (pH 7.3) for 3 min at 25°C. Immunolabeling was not substantively altered by increasing the time of sodium metaperiodate preincubation or by substituting a colloidal gold/donkey anti-rabbit IgG detection system (43).

Analytical methods

Bile flow was determined gravimetrically, assuming a specific gravity of 1.0. Total 3α-hydroxy-bile salt output was assayed with 3α-hydroxysteroid dehydrogenase (44); preliminary studies demonstrated that the taurine conjugate of 3α-hydroxy-7,12-keto-5β-cholanoic acid (the principal biliary metabolite of TDHC) was detected quantitatively. Phospholipid and cholesterol were assayed by standard methods (28). Biliary bile salt composition was measured by HPLC-electrospray ionization mass spectrometry, using known standards (29).

Statistical analysis

Digital morphometry was performed to determine the area and width of each bile canaliculus and the dimensions of structural profiles. Using StatPak software (Northwest Analytical, Portland, OR), comparisons among experimental animals were made using one-way analysis of variance (ANOVA) followed by Newman-Keuls multiple range tests for pairwise comparisons (45).

RESULTS

Chemically fixed liver tissue

Bile canaliculi in chemically fixed tissue (see Methods), as imaged by conventional transmission electron microscopy (TEM), are shown in **Fig. 1a–f.** In the lumena of bile canaliculi of control animals (Fig. 1a), unilamellar vesicles were consistently observed along with occasional larger membranous structures (Fig. 1b). Vesicle diameters in the canaliculi of control animals were 63 ± 17 nm (± SD, range 20–100 nm, n = 268), with zero to > 50 vesicles per canaliculus. Vesicles were observed rarely in bile canaliculi of bile salt-depleted rats (Fig. 1c) but were present in bile salt-depleted animals infused with TC (Fig. 1d).

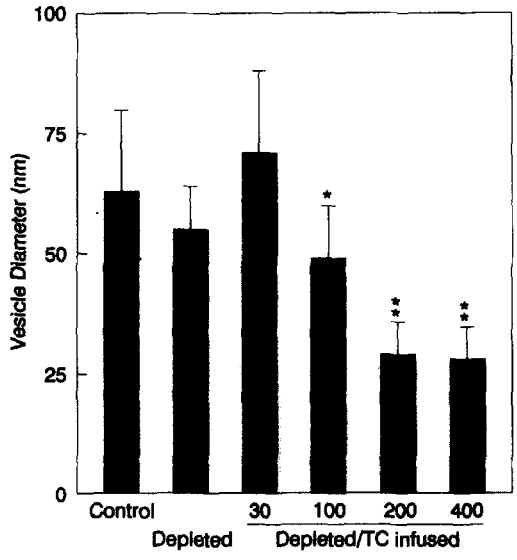

Fig. 2. Diameter of vesicles in chemically fixed liver tissue. Depicted on the abscissa are vesicle diameters (in nm, ± SD) from bile canaliculi of two control rats, one bile salt-depleted rat, and bile salt-depleted rats infused 1 h with TC at different rates (n = 2 each). Vesicle sizes are smaller at higher TC infusion rates. Total number of vesicles measured were 268, 25, 21, 52, 43, and 37 for each successive (left to right) vertical bar. $*P < 0.05$, $**P < 0.01$ vs. control animals.

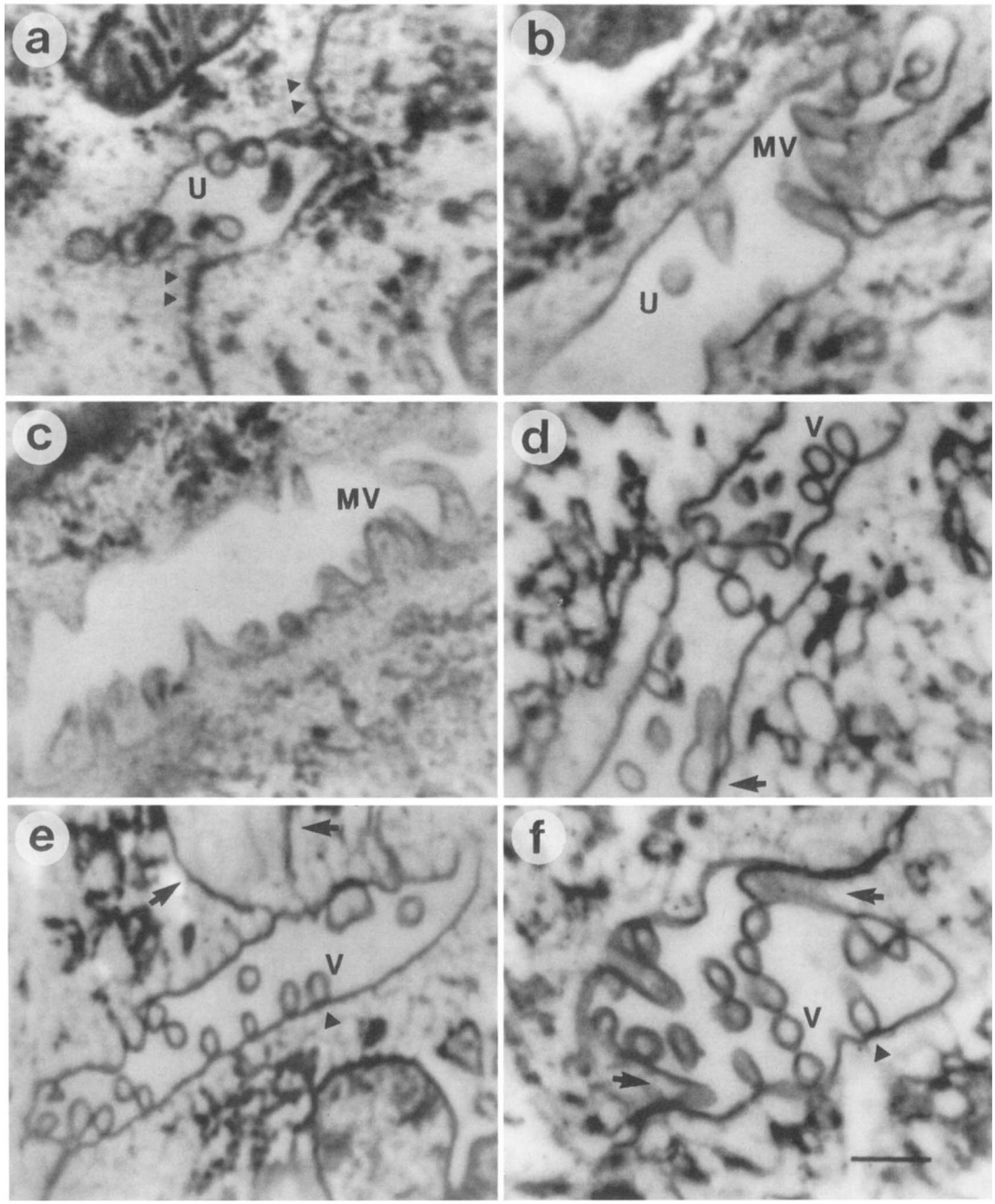

Fig. 3. Electron spectroscopic imaging of bile canaliculi from cryofixed liver. Images are shown from (a) control and (b) bile salt-depleted rats, and from depleted rats infused with (c) TDHC, (d) TUC, (e) TUDC, and (f) TCDC at 200 nmol/min per 100 g. Bile canaliculi were delimited by tight junctional zones; denoted in (a) by arrowheads. In panels (b) and (c), canaliculi contained microvilli (MV), with faint electron-dense contents and basal continuity with the cytoplasm. Circular or ellipsoid structures with faint electron-dense contents were denoted "uncertain" (U; panels a and b, see text). Panels (d), (e), and (f) show distinct vesicles (V) with sharp membrane borders. Vesicles were free within the lumen or attached to the canalicular membrane along linear zones of contact (arrow heads; panels e and f). Panel (d) shows a rare larger membranous structure affixed to the canalicular membrane (arrow). Panel (e) contains a lateral extension of the canalicular membrane in the form of an outpouch (arrows; ref. 47). Panel (f) shows microvilli closely apposed to the tight-junctional region (arrows, a.k.a. "marginal ridges" (48)). All images are shown at the same magnification, except for (e), which is 33% reduced. Bar for (a–d, f) = 200 nm.

Virtually all vesicles were free within the canalicular lumena; rare vesicles were adherent to canalicular membranes (Fig. 1e). A multilamellar luminal vesicle was observed only once (Fig. 1f). **Figure 2** shows that vesicle diameters were 60–70 nm in bile salt-depleted rats infused with TC at 30 nmol/min per 100 g. However, at the higher infusion rates, vesicle diameters were significantly smaller.

When rats were infused with TC, steady state bile salt secretion rates were equivalent to infusion rates, and TC constituted >96% of secreted bile salts at TC infusion rates ≥ 200 nmol/min per 100 g. Phospholipid and cholesterol secretion rates plateaued at ~50 and ~0.8 nmol/min per 100 g, respectively. These values were similar regardless of whether animals were fasted or fed prior to experimentation (data not shown).

Cryofixed liver tissue

The terminal illness of G-M. M. led to a time gap of several years in these studies. Upon resumption, ultrarapid cryofixation techniques had become available (37). Liver tissue was obtained from control and bile salt-depleted animals and from the latter animals infused with bile salts at 200 nmol/min per 100 g. Because biliary lipid secretion is influenced by the physicochemical properties of bile salts (13, 46), we infused rats with common bile salts and synthetic congeners spanning a wide hydrophobicity range.

Excellent ultrastructural preservation of liver tissue was achieved, enabling ready identification of bile canaliculi (**Fig. 3a**), although images were coarser when compared with conventional TEM (Fig. 1). As shown in Fig. 3a–f, three groups of intracanalicular structural profiles were observed. Microvilli (Fig. 3b, c) were identified as elongated structures having a delimiting membrane in continuity with the canalicular plasma membrane and a faint electron dense core in continuity with the cytoplasm. Vesicles (Fig. 3d–f) were distinguished by sharp membrane outlines, and electron-lucent interiors separated from the cytoplasm by a thicker membrane. Most vesicles were adherent to the external aspect of the canalicular membrane, exhibiting abrupt angular junctions (Fig. 3d–f). No vesicular structures were observed affixed to the canalicular membrane on the cytoplasmic side. A population of uncertain structures were identified as circular or ellipsoid profiles with faint electron-dense interiors (Fig. 3a, b). Although these structures most likely represented microvilli cut in cross section, some vesicles may have been included.

Morphometric analysis

Results obtained from measurements of 254 bile canaliculi and 3,019 structural profiles are presented in **Table 1.** Numerous vesicles were identified in the control, suckling, and bile salt-depleted animals infused with micelle-forming bile salts (TUC, TMC, TUDC, TC, and TCDC). In contrast, vesicles were rare in the bile salt-depleted and TDHC-infused animals. In the seven animals with abundant vesicles, the majority of vesicles were adherent to the canalicular membrane (247/333, 77 ± 12%, ± SD, n = 7); many canaliculi were devoid of vesicles (88/195, 40 ± 17%).

The dimensions of vesicles, mixed structures, and microvilli were remarkably constant in size, with no significant differences between groups. The size distributions of canalicular structures by electron spectroscopic imaging are shown in **Fig. 4.** Vesicles and uncertain structures exhibited minimal and maximal dimensions of 40 to 120 nm, whereas microvilli approached 300 nm in maximal dimensions. Overall, vesicles exhibited minimum dimensions of 67 ± 13 nm (± SD, n = 341), maximum dimensions of 86 ± 16 nm, and areas of 4437 ± 763 nm^2.

Bile canalicular areas were generally less than 1 μm^2 (Table 1). Canalicular width (perpendicular to the long axis) was generally 0.3–0.5 μm, which is smaller than that reported for chemically fixed tissue (49) or for hepatocyte couplets (23). The only canaliculi exceeding 0.5 μm in width were those of the TDHC-infused rat (ascribed to TDHC-induced choleresis (47)) and the TCDC rat, possibly related to cholestasis (discussed below). An average of 1 to 3 vesicles was observed per canaliculus in the control and in rats infused with common bile salts; this value was greatly reduced in the bile salt-depleted and TDHC-infused rats, with the suckling rat exhibiting an intermediate value. Vesicles occupied 1.7–2.5% of bile canalicular area, with lower values in the suckling rat (0.8%) and bile salt-depleted and TDHC-infused rats (≤ 0.2%, $P < 0.02$ vs. control). Microvilli occupied between 12 and 24% of canalicular area. The highest microvillus occupancy occurred in the bile salt-depleted rat, in keeping with the findings in chemically fixed tissue (Fig. 1c). The number and % area of uncertain structures did not vary significantly among the nine experimental groups, suggesting that the majority of uncertain structures were cross-sectioned microvilli.

Supplemental measurements were performed on the 333 vesicles in the seven rats with abundant vesicles. Among the 247 adherent vesicles, the long axis was perpendicular (± 15°) to the canalicular membrane in 214 (85 ± 8%, ± SD, n = 7) and the axial ratio (width/perpendicular length) was 0.80 ± 0.19 ($P < 0.0001$ vs. unity), corroborating the oblong shape (Fig. 3). The 86 non-adherent vesicles exhibited aspect ratios of 0.81 ± 0.12, also different ($P < 0.0001$) from unity.[4] The linear membranes at the base of adherent vesicles were 20 ± 5 nm thick (± SD, n = 247), significantly thicker ($P < 0.0001$)

[4]Freeze-drying is an unlikely source of artefactual vesicle adherence and ovoid shape, as it would not have generated the perpendicular orientation nor the distinct junction observed between vesicles and canalicular membrane (Figs. 3). Furthermore, mechanical compression was an unlikely cause, as the axial ratio was unrelated to orientation of the specimen.

TABLE 1. Morphometric analysis of cryofixed bile canaliculi

Parameter	Units	Control	Suckling	Depleted	TDHC	TUC	TMC	TUDC	TC	TCDC
Counts of structures										
Bile canaliculi	#	20	38	36	23	24	23	22	30	38
Vesicles	#	23	23	2	6	55	61	23	48	100
Uncertain structures	#	38	38	45	26	63	40	35	40	101
Microvilli	#	105	308	349	235	143	219	59	235	599
Adherent vesicles	#	21	17	1	3	39	52	21	30	67
Adherent vesicles	%	91	74	50	50	71	85	91	63	67
Canaliculi without vesicles	#	11	23	34	19	13	7	15	12	7
Canaliculi without vesicles	%	55	61	94	83	54	30	22	40	18
Primary measurements[a]										
Minimum dimension	nm									
Vesicles		64 ± 15	79 ± 11	61 ± 1	52 ± 8	64 ± 12	72 ± 12	61 ± 11	65 ± 10	72 ± 12
Uncertain structures		64 ± 15	79 ± 12	70 ± 14	61 ± 14	59 ± 13	71 ± 12	55 ± 11	67 ± 16	71 ± 12
Microvilli		67 ± 14	86 ± 27	75 ± 19	64 ± 17	67 ± 15	79 ± 23	64 ± 17	70 ± 19	79 ± 23
Maximum dimension	nm									
Vesicles		77 ± 17	98 ± 17	76 ± 5	71 ± 17	87 ± 16	92 ± 15	79 ± 14	81 ± 14	92 ± 15
Uncertain structures		79 ± 17	96 ± 15	81 ± 16	80 ± 13	81 ± 17	122 ± 22	73 ± 19	89 ± 16	122 ± 22
Microvilli		136 ± 64	196 ± 63	159 ± 81	150 ± 80	144 ± 60	160 ± 71	126 ± 47	138 ± 59	160 ± 71
Area/structure	$nm^2 \div 100$									
Vesicles		41 ± 3	53 ± 17	37 ± 4	32 ± 6	48 ± 2	57 ± 15	40 ± 3	43 ± 13	57 ± 15
Uncertain structures		45 ± 18	59 ± 18	42 ± 18	36 ± 12	49 ± 19	53 ± 18	53 ± 39	47 ± 18	53 ± 18
Microvilli		79 ± 16	97 ± 90	105 ± 73	75 ± 61	98 ± 90	97 ± 57	74 ± 43	74 ± 51	97 ± 52
Derived measurements[b]										
Bile canaliculi										
Area	μm^2	0.34 ± 0.07	0.71 ± 0.62[c]	0.40 ± 0.07	0.64 ± 0.11[c]	0.52 ± 0.09	0.45 ± 0.11	0.21 ± 0.03	0.41 ± 0.27	0.85 ± 0.11
Width	µm	0.34 ± 0.04	0.39 ± 0.03	0.43 ± 0.05	0.52 ± 0.05[d]	0.47 ± 0.05	0.33 ± 0.03	0.26 ± 0.03	0.42 ± 0.03	0.59 ± 0.03
Number/canaliculus										
Vesicles	#	1.2 ± 0.3	0.6 ± 0.1	0.1 ± 0.0[d]	0.3 ± 0.1[d]	2.3 ± 0.8	2.6 ± 0.5	1.1 ± 0.6	1.5 ± 0.3	2.6 ± 0.6
Uncertain structures	#	1.9 ± 0.4	1.0 ± 0.0	1.3 ± 0.2	1.1 ± 0.3	2.6 ± 0.5	2.7 ± 0.5	1.6 ± 0.5	1.3 ± 0.3	2.7 ± 0.5
Microvilli	#	5.3 ± 1.2	16 ± 8	10 ± 1	10 ± 2	6.0 ± 0.9	10 ± 1	2.7 ± 0.4	7.8 ± 0.7	16 ± 2
Aggregate % area/canaliculus										
Vesicles	%	2.4 ± 0.9	0.8 ± 0.2	0.1 ± 0.1[d]	0.2 ± 0.1[d]	1.8 ± 0.6	2.5 ± 0.6	1.7 ± 0.8	2.4 ± 0.6	1.9 ± 0.4
Uncertain structures	%	3.8 ± 0.8	0.9 ± 0.2	1.9 ± 0.5	1.4 ± 0.1	3.0 ± 0.5	1.7 ± 0.3	3.4 ± 0.8	2.0 ± 0.6	1.7 ± 0.3
Microvilli	%	19 ± 3	12 ± 1[d]	24 ± 2	13 ± 2[d]	15 ± 2	18 ± 2[d]	12 ± 2	17 ± 2	20 ± 1

Canalicular lumenal structures defined as follows: vesicles, unilamellar ellipsoid or circular structures with sharp outlines and electron-lucent interiors; uncertain structures, circular or ellipsoid structures with electron-dense interiors; microvilli, elongated structures with a delimiting membrane in continuity with the canalicular membrane and electron-dense interiors in continuity with the pericanalicular cytoplasm. TDHC, taurodehydrocholate; TUC, tauroursocholate; TMC, tauromurichолate; TUDC, tauroursodeoxycholate; TCDC, taurochenodeoxycholate. Each column represents results from one animal.

[a]Values ± SD.

[b]Values ± SEM.

[c]$P < 0.01$ versus control.

[d]$P < 0.02$ versus control.

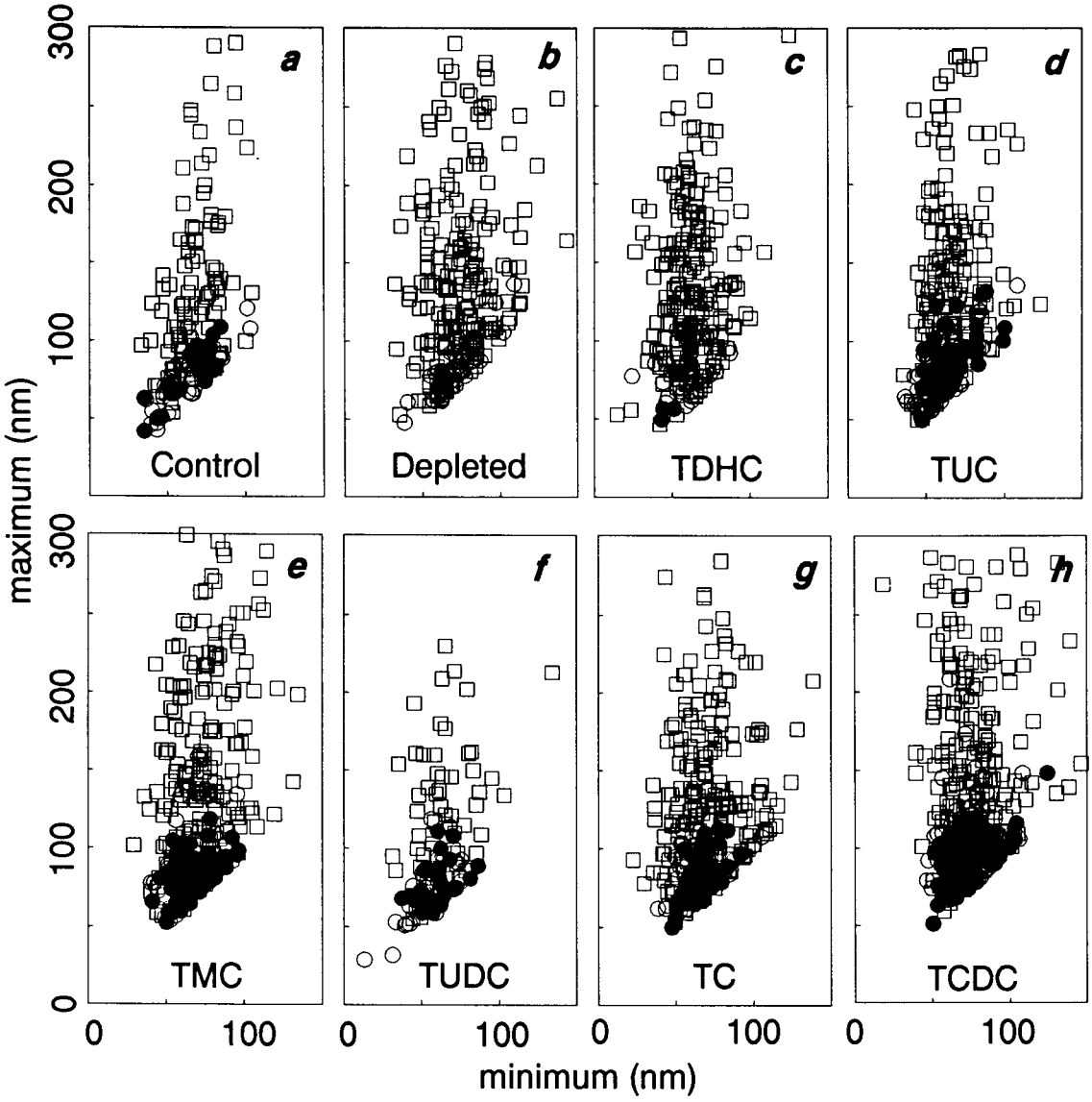

Fig. 4. Dimensions of structural profiles in bile canaliculi. The minimal and maximal dimensions are shown for all vesicles (closed circles), uncertain structures (open circles), and microvilli (open squares) measured in bile canaliculi of adult rats: (a) control, (b) bile salt-depleted, (c) TDHC, (d) TUC, (e) TMC, (f) TUDC, (g) TC, and (h) TCDC-infused (n = 1 animal in each instance).

than the top of vesicles and adjacent canalicular membrane (both 12 ± 2 nm).

Biliary lipid secretion

Table 2 lists steady state bile flow, bile salt, and phospholipid secretion rates for the bile salt-depleted and depleted/bile salt-infused animals utilized for cryofixation studies. In bile salt-infused animals, bile flow was 4–10 μl/min per 100 g and bile salt secretion rates were 39–210 nmol/min per 100 g, with partial elimination of hydrophilic bile salts (particularly TDHC metabolites) via urinary excretion (29). Phospholipid secretion rates were 8–47 nmol/min per 100 g and increased with increased hydrophobicity of the infused bile salt (TDHC = TUC < TMC < TUDC < TC, not including TCDC), correlating inversely with bile flow (r = 0.803, $P < 0.05$). Bile salt and phospholipid secretion rates were lowest in the bile salt-depleted animal and the TCDC-infused animal, the latter due to progressive cholestasis (13).

The major bile salts secreted by the depleted and suckling animals were TC and TMC, with minor contributions from taurine-conjugated dihydroxy bile salts and glycine-conjugated bile salts (not shown); a similar distribution has been observed in control animals (29). Infused TDHC was quantitatively reduced at the 3-position, and was secreted as taurine-conjugated dioxo-monohydroxy, monooxo-dihydroxy, and trihydroxy

TABLE 2. Bile flow and lipid cutput prior to cryofixation

Measurement	Depleted	TDHC	TUC	TMC	TUDC	TC	TCDC
Bile flow, μl/min/100 g	5.5	9.9	9.8	8.3	6.5	7.2	3.6
Bile salt output, nmol/min/100 g	17	89	164	157	172	210	39
Phospholipid output, nmol/min/100 g	3	13	12	22	29	47	8

Bile was collected over the final 15 min prior to liver harvesting for animals presented in Tables 1 and 2 (one animal per column). Bile salt and phospholipid outputs represent the means of quadruplicate determinations.

(principally TC) metabolites. Other infused bile salts comprised ≥ 91% of those recovered in bile; some trihydroxy metabolites (TMC and TC) were present in the TCDC-infused animal.

Phospholipid secretion rates (means of the TUC, TMC, TUDC, and TC-infused rats, Table 2) were used to obtain an order-of-magnitude estimate of the expected number of vesicles in bile canaliculi (see Appendix), based on the concept that the observed vesicles were composed predominantly of phospholipid molecules. This calculation utilized mean values for vesicle diameter and bile canalicular area (Table 1), and a molecular area of ~ 46 $Å^2$ for close-packed phosphatidylcholine molecules (50). We estimated 2.0 ± 1.1 vesicles/canaliculus, which was in excellent agreement with the observed 1.9 ± 0.7 vesicles/canaliculus (see Appendix). These calculations suggest that the membrane surface area of vesicles present in bile canaliculi is sufficient to account for all phospholipid molecules in hepatic bile.

Immunoelectron microscopy

Because physicochemical studies (13) reveal a very high CMC for TUC and hence membrane vesicles should undergo the least remodeling in the canaliculus, tissue sections from the TUC-infused rat were selected for immunogold electron microscopy. **Figure 5** shows that immunogold labeling with antibodies to actin resulted in gold deposition over the tight junctional region and microvilli. Labeling with antibodies to a 100 kDa ectoATPase canalicular membrane protein was limited to the immediate vicinity of the canalicular membrane and microvilli (51). **Figure 6** presents the immunogold labeling of bile canaliculi in histogram format. The pericanalicular cytoplasm, microvilli, and canalicular membrane were labeled with anti-actin. Anti-ectoATPase labeled microvilli and the canalicular membrane between microvilli and to some extent the pericanalicular cytoplasm. When vesicles (V) and uncertain structures (U) were scored as one group, they were found to be labeled only once with anti-ectoATPase and never with anti-actin antibodies. Thus, vesicles that might be included in this group exhibited essentially no immunoreactivity for these antigens.

DISCUSSION

Secretion of bile is the quantitative means by which vertebrates eliminate cholesterol and many hydrophobic xenobiotics, and is critical for the efficient digestion and absorption of dietary lipid. Elucidation of the physical-chemical and biological mechanisms for hepatic phospholipid secretion is central to understanding how bile is elaborated. In this study, we provide ultrastructural evidence that unilamellar lipid vesicles form on the external surface of the canalicular plasma membrane and are released into canalicular bile. Although the exact vesiculation mechanism is not revealed, our observations provide new information that corroborates the following proposed sequence of events for biliary phospholipid secretion: cytosolic delivery of intracellular phosphatidylcholine molecules to the internal hemileaflet of the canalicular membrane possibly via binding to PC-TP (3); phospholipid transfer from the internal to the external hemileaflet of the canalicular membrane most likely through the action of one or more transmembrane translocators (5, 7, 8, 52); and formation and detachment of unilamellar vesicles from the canalicular membrane, presumably mediated by the detergent action of luminal bile salts (11).

Visualization of vesicle formation

Our data provide insights into why vesicular secretion events have not previously been visualized. First, even with physiological phospholipid secretion rates, we show experimentally (Table 1) and by calculation (see Appendix) that 50-nm thin sections through canaliculi contain an average of 1 to 3 vesicles only, and up to 60% of canalicular lumena in thin sections are devoid of vesicles (Table 1). Second, classical chemical fixation is a diffusion-limited process which takes several seconds (32) as opposed to metal-mirror cryofixation which arrests cellular function and physical-chemical processes within milliseconds (53). As virtually all canalicular ves-

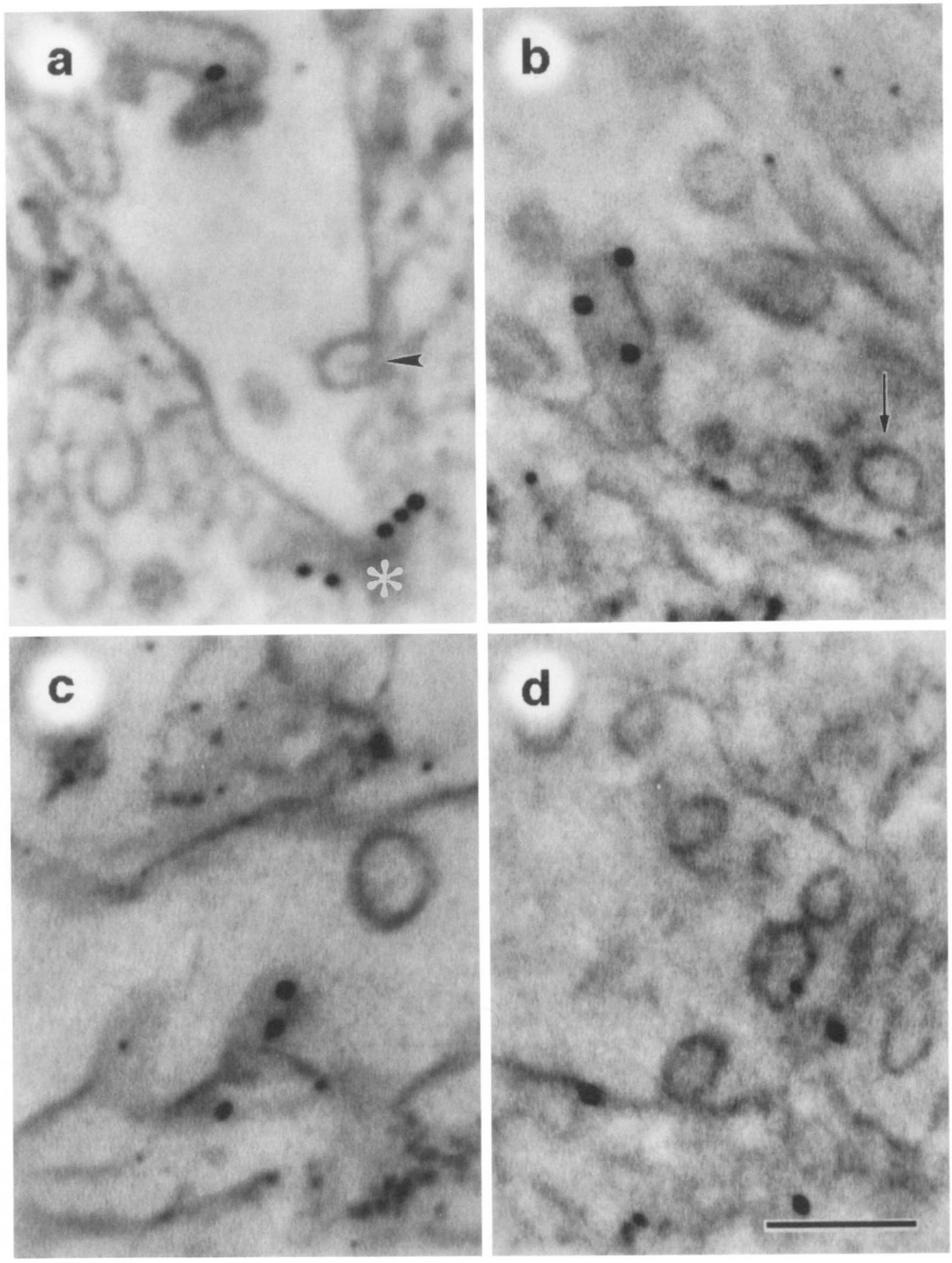

Fig. 5. Immunoelectron microscopy for actin and canalicular membrane 100 kDa ecto/ATPase. Immunogold labeling (10 nm particles, see Methods) with anti-actin (a, b): gold particles are present within microvilli and in the pericanalicular tight junctional region (asterisk); an adherent vesicle (arrowhead) and free vesicle (arrow) are free of 10 nm particles. Immunogold labeling with anti-ectoATPase (c, d): the canalicular membranes and microvilli show labeling for the ectoATPase, but ellipsoid luminal structures do not. The smaller black dots (< 5 nm in diameter) are normally observed in cryofixed hepatocytes imaged at high magnification by electron spectroscopic imaging (37), and do not represent immunogold labeling. Bar = 200 nm applies to all panels.

icles in chemically fixed liver tissue were free within the lumena (Fig. 1), compared to only 23% of vesicles in cryofixed tissue (Fig. 3 and Table 1), it appears that vesicle formation and detachment occur on a rapid time frame. In fact, it is known that peak biliary secretion of an i.v. bile salt bolus slightly precedes secretion of biliary

phospholipid (54). Third, secreted vesicles are unstable in the canalicular lumen in the presence of bile salts. The low millimolar bile salt concentrations in canalicular bile (23) are capable of dissolving lipid vesicles into mixed micelles over a period of minutes (55). As aldehyde fixation does not stabilize membrane lipids (56), micellar bile salts retained in the canalicular space will promote complete vesicle dissolution. Early introduction of osmium, as in our chemical fixation protocol, stabilizes membrane structures earlier (56), although not without some reduction in vesicle diameter at high bile salt secretion rates (Fig. 2).

Although cryofixation techniques are not free of artefact, we can offer persuasive evidence that canalicular vesicles do not arise from fixation artefact. Rapid decreases in temperature may cause deformation of membrane structure during cryofixation (57); however, membrane ripples are flattened (57) rather than accentuated, and adherent vesicles are not generated. It is possible, nevertheless, that the base of adherent vesicles may have broadened during contraction of the surrounding canalicular membrane (58). The presence of canalicular vesicles in cryofixed tissue also indicates that they are not an artefactual result of aldehyde fixation (59). However, the luminal multilamellar figures observed in chemically fixed tissue (Fig. 1f and ref. 15) may be artefactual (60), as they were not observed in cryofixed bile canaliculi.

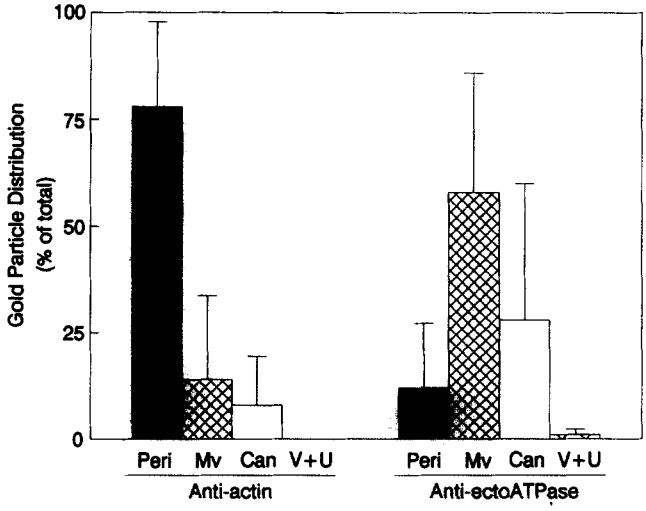

Fig. 6. Distribution of immunogold particles. Immunogold labeling using anti-actin IgG and anti-ectoATPase serum on sections from the TUC-infused rat is shown as a percentage (± SD) of all gold particles in each bile canalicular image. Abbreviations: Peri, pericanalicular domain, defined as a radius of 0.5 μm around the bile canaliculus and including the tight junctional region; Mv, microvilli; Can, canalicular membrane between microvilli; V + U, combined score for vesicles and uncertain structures. For anti-actin, n = 31 bile canaliculi and 367 gold particles. For anti-ectoATPase, n = 8 bile canaliculi and 46 gold particles.

Vesicle diameters in canaliculi of cryofixed livers were identical regardless of the hydrophobicity of infused bile salt within the range studied (Table 1), an observation noted previously (13). Moreover, the fact that we observed no nascent vesicles smaller than 40 nm diameter is in keeping with the report (55) that vesicles of smaller diameter, and hence greater curvature, are unstable even in the presence of bile salt monomers and rapidly reorganize into vesicles of a size comparable to that seen in this study. Vesicle % occupancy did not vary significantly among animals infused with TUC, TMC, TUDC, TC, and TCDC (Table 1) despite marked differences in bile salt hydrophobicity (46) and phospholipid coupling (Table 2). In addition, phospholipid output was similar in the TDHC and TUC-infused rats, despite differences in vesicle % occupancy. A possible explanation for both dichotomies lies in the inverse correlation between phospholipid secretion rates and bile flow in these animals (see Results). Morphological images are static and do not provide information on the rate at which vesicles form and are released. Enhanced bile flow with more hydrophilic bile salts operates in parallel with decreased rates of phospholipid secretion (11). Thus, vesicle "occupancy" will reflect the balance between vesicle formation, their removal by flow, and dissolution by micellar bile salts. In particular, substantial differences in the detergency and micelle-forming capacity of the oxo-hydroxylated metabolites of TDHC versus TUC may contribute to these observations.

Our immunoelectron microscopic results (Figs. 5 and 6) suggest that vesicles lack two proteins found in the surrounding canalicular region, actin and a canalicular 100 kDa ectoATPase. Immunoreactivity herein was less than that reported for conventionally processed tissue (43, 51, 61), possibly the result of using an epoxy resin (62) or osmium (63). The use of Spurr resin was dictated by the necessities of allowing permeation of tissue that had been completely dehydrated. Light exposure to osmium (as in this study and in ref. 37) enables successful immunolocalization of antigens (64) with or without pretreatment with sodium metaperiodate to remove excess osmium (42, 64). Despite decreased overall immunoreactivity, actin and the 100 kDa canalicular protein were labeled in the expected pericanalicular, microvillus, and canalicular membrane domains, similar to other reports (43, 51, 61, 65, 66).

Previous hypotheses for canalicular lipid secretion

Prior models to account for canalicular lipid secretion include: *1)* bilayer plasma membrane vesiculation, as proposed for "fusion-budding" (67) or "pinching-off" (9) of canalicular membrane patches; *2)* release of preformed unilamellar lipid vesicles via fusion of multivesicular bodies with the canalicular membrane (67);

3) interaction of bile salts with loosely bound phospholipid and cholesterol during bile salt transit through canalicular membrane "soft-gate" (10, 68); and *4)* secretion of monomeric bile salts followed by their interaction with the external aspect of the canalicular membrane (11, 69).

The first three possibilities can be dismissed readily. Possibility 1 should promote release of cytoplasmic enzymes (aminotransaminases and lactate dehydrogenase) into bile. Such enzyme release remains at very low levels (70), unless elevated during hepatic exposure to toxic levels of bile salts (71) or to agents that disrupt normal phospholipid secretion (72). Moreover, membrane exocytosis was not observed in this study. Possibility 2 would require the presence of pericanalicular multivesicular bodies, whereas pericanalicular unilamellar vesicles increase during bile salt choleresis (36). Although we have postulated in the past that such intracellular vesicles may promote delivery of biliary lipid to the canalicular membrane (28), more recent evidence suggests that they play a primary role in delivering proteins and structural lipid to the canalicular membrane (29, 51, 73–75). The sensitivity of biliary lipid secretion to agents that disrupt Golgi and cytoskeletal function (4, 9, 28, 72) may thus be due to impaired cellular delivery of relevant transport proteins to the canalicular membrane. Possibility 3 is unlikely as bile salts are transported across the canalicular membrane bilayer by specific transport proteins (1). Moreover, secreted organic anions may interact with intraluminal bile salts and thereby inhibit bile salt-induced biliary lipid secretion (9, 76).

Instead, our findings support hypothesis 4, and suggest that vesicles arise via luminal bile salt-induced vesiculation of lipid microdomains in the exoplasmic hemileaflet of the canalicular membrane. This conclusion is based on our ultrastructural demonstration that: *1)* a membrane barrier is maintained between cytosol and vesicle interiors; *2)* adherent vesicles exhibit a sharply demarcated zone of contact with the external aspect of the membrane which is thick and linear; *3)* cytoplasmic actin and a canalicular membrane protein appear to be excluded from the vesicles; and *4)* realistic calculations (see Appendix) suggest that a vesicular secretion mechanism is sufficient to account for all secreted phospholipid molecules in hepatic bile.

Conclusions

We have provided ultrastructural evidence that biliary phospholipid molecules are secreted by hepatocytes as unilamellar vesicles arising from the external aspect of the canalicular plasma membrane. Documentation of the secretion process required ultrarapid cryofixation techniques; chemical fixation of liver tissue confirmed the existence of lipid vesicles within canalicular lumena. Vesicles averaged 63–67 nm in diameter and were observed primarily in the canaliculi of normal animals or in animals secreting infused bile salts after depletion of endogenous pools. Vesicles appeared to be free of actin and a canalicular membrane 100 kDa ecto-ATPase. Our findings lend support to the proposal that protein-mediated phospholipid translocation from the internal to external hemileaflet of the canalicular membrane (8) exposes biliary-type phosphatidylcholine to the detergent action of luminal bile salts (11).

Because the mechanical events leading to membrane topological reorganization occur on a microsecond timescale (77), the transitions from pre-existing canalicular membrane to nascent vesicles were not captured in the millisecond time frame of cryofixation (53). Thus, the physicochemical mechanisms responsible for vesicle formation remain speculative. It also should be noted that cholesterol (20, 21, 78) and low levels of intrinsic canalicular membrane proteins (e.g., aminopeptidase N and 5′-nucleotidase (14, 15, 20–22, 72)) are normally found in association with biliary lipid vesicles. Future studies will be required to determine whether cholesterol and protein are secreted in association with lipid vesicles, and whether protein secretion is dependent on exovesiculation of one or both hemileaflets of the canalicular membrane bilayer. Delineation of the exact events leading to vesiculation of membrane phospholipid and apparent cosecretion of cholesterol and certain proteins must await future investigation along these lines. Elucidation of these mechanisms will be crucial for understanding how hepatic lipid is secreted normally in humans, and how gallstone disease is initiated by hepatic secretion of cholesterol-supersaturated bile (10). ■

We thank Rebecca C. Stearns, Carol Allan, and Caroline Snowman for their expert technical assistance, and Drs. Ann L. Hubbard and David E. Cohen for their helpful criticisms during the course of these studies. Dr. Bernard J. Ransil kindly performed on the PROPHET system (National Center for Research Resources, National Institutes of Health) calculations to evaluate vesicle density overestimates deduced from morphometric measurements. Special thanks are due to Dr. Jerry S. Trier, Director of the Morphology Core of the Harvard Digestive Diseases Center, for making available his facilities used in the chemical fixation studies. This study was supported by NIH grants DK-44981 (JMC), DK-39512 (JMC), and DK-36588 (MCC), and with the support of the Morphology and Membrane Core Units of the Harvard Digestive Diseases Center (DK-34854). The experiments reported herein were conducted according to the principles set forth in the "Guide for the Care and Use of Laboratory Animals", Institute of Animal Resources, National Research Council. Portions of this work have been presented in abstract form at the annual meeting of the American Gastroenterological Association, May, 1994 (*Gastroenterology.* **106:** A879), and at the XIIIth International Bile Acid Symposium, San Diego, CA, September, 1994.

Manuscript received 20 March 1995 and in revised form 29 June 1995.

APPENDIX: ESTIMATED NUMBER OF VESICLES IN BILE CANALICULI

The phospholipid secretion rates of the TUC, TMC, TUDC, and TC-infused animals (Table 2) were used to obtain an order-of-magnitude estimate of the expected number of secreted vesicles in a bile canaliculus, as follows:

TABLE 3. Estimated vesicle numbers in bile canaliculi

Phospholipid molecules per vesicle	
Area of a sphere	$4 \pi r^2$
Radius of vesicles (average ± SD of TUC, TMC, TUDC, TC, Table 1)	33 ± 2 nm
Phosphatidylcholine molecular area	46 Å^2
Hemileaflets per vesicle	2
Phospholipid molecules per vesicle	$6.0 \pm 0.4 \times 10^4$
Phospholipid molecules in bile	
Phospholipid secretion rate (average ± SD of TUC, TMC, TUDC, TC, Table 2)	28 ± 14 nmol/min/100 g
Bile flow (average ± SD of TUC, TMC, TUDC, TC, Table 2)	8 ± 1 µl/min/100 g
Phospholipid concentration (nmol)	3.7 ± 2.3 nmol/µl
Phospholipid concentration (molecules)	$2.3 \pm 1.4 \times 10^{15}$ molecules/µl
Phospholipid concentration (vesicles)	$3.8 \pm 2.4 \times 10^{10}$ vesicles/µl
Estimated canalicular vesicle content	
Bile canalicular area (average ± SD of TUC, TMC, TUDC, TC; Table 1)	0.4 ± 0.1 µm^2
Sectional canalicular volume (50 nm section)	$2.0 \pm 0.7 \times 10^{-11}$ µl
Predicted vesicle content	0.8 ± 0.5 vesicles/canaliculus
Revised assumptions[a]	0.9 ± 0.5 vesicles/canaliculus
Adjustment for 2-dimensional overestimate[b]	2.0 ± 1.1 vesicles/canaliculus
Observed canalicular vesicle content (average ± SD of TUC, TMC, TUDC, TC, Table 1)	1.9 ± 0.7 vesicles/canaliculus

[a]The assumptions made in this calculation are: *1)* bile is not modified by extraction or secretion of lipid or fluid in the post-canalicular biliary tree; *2)* vesicles are composed entirely of phospholipid; *3)* vesicles are spherical; *4)* the surface area of a fully hydrated but close-packed phosphatidylcholine molecule is ~46 Å^2 (50); and *5)* the internal hemileaflet of each vesicle membrane contains ~11% fewer phospholipid molecules than the external hemileaflet due to membrane curvature. Assumptions 1–3 are revised as, under normal conditions, *1)* bile duct epithelial cells generate an aqueous electrolyte secretion accounting for ~25% of bile water, *2)* vesicles contain about 14% molar cholesterol (see Results and (15, 78, 79), and *3)* the surface area of ovoid particles is about 26% greater than that of spheroid particles of the same minimum dimension. A revised estimate of 0.9 ± 0.5 vesicles per canaliculus is obtained.

[b]An overestimate in "observed" vesicles viewed in 2-dimensions in a sampled volume versus actual vesicles per unit volume is encountered when vesicle diameter exceeds the section thickness (80). The magnitude of this discrepancy was calculated by two independent methods. First, 50-nm sections cannot fully encompass vesicles of minimum diameter greater than 50 nm. The thickness (and hence volume) required to encompass all vesicles in each section was computed for each canaliculus, and the ratio of "encompassing volume"/"actual volume" was compiled for each animal. This calculation indicated that vesicle content was overestimated in the TUC, TMC, TUDC, and TC rats by 2.1 ± 0.4-fold (±SD). Second, the entire surface area of vesicles larger than 50 nm will not be included in sections 50-nm thick; only vesicles ≤ 50 nm in minimum dimension are fully encompassed. For each larger ovoid vesicle, computing the ratio (surface area of ovoid vesicle ≥ 50 nm minimum diameter)/(surface area of 50 nm sphere) suggests an overestimate of vesicle density of 2.3 ± 0.2-fold. Thus, the observed 1.9 ± 0.7 vesicles/canaliculus in the 50-nm sections is likely to differ ~2.2-fold from the content estimated from volumetric data (phospholipid secretion rate). Adjusting for this difference yields a correlation between estimated and observed vesicle content which is highly satisfactory.

REFERENCES

1. Suchy, F. J. 1993. Hepatocellular transport of bile acids. *Semin. Liver Dis.* **13:** 235–247.
2. Patton, G. M., J. M. Fasulo, and S. J. Robins. 1994. Hepatic phosphatidylcholines: evidence for synthesis in the rat by extensive reutilization of endogenous acylglycerides. *J. Lipid Res.* **35:** 1211–1221.
3. Cohen, D. E., M. R. Leonard, and M. C. Carey. 1994. In vitro evidence that phospholipid secretion into bile may be coordinated intracellularly by the combined actions of bile salts and the specific phosphatidylcholine transfer protein of liver. *Biochemistry.* **33:** 9975–9980.
4. McIntyre, J. C., and R. G. Sleight. 1994. Mechanisms of intracellular membrane lipid transport. *Curr. Top. Membr.* **40:** 453–481.
5. Oude Elferink, R. P. J., R. Ottenhoff, M. van Wijland, J. J. M. Smit, and A. H. Schinkel. 1995. Regulation of biliary lipid secretion by mdr2 P-glycoprotein in the mouse. *J. Clin. Invest.* **95:** 31–38.
6. Higgins, C. F. 1994. To flip or not to flip? *Curr. Biol.* **4:** 259–260.
7. Berr, F., P. J. Meier, and B. Stieger. 1993. Evidence for the presence of a phosphatidylcholine translocator in isolated rat liver canalicular plasma membrane vesicles. *J. Biol. Chem.* **268:** 3976–3979.
8. Smit, J. J. M., A. H. Schinkel, R. P. J. Oude Elferink, A. K. Groen, E. Wagenaar, L. Van Deemter, C. A. A. M. Mol, R. Ottenhoff, N. M. T. Van der Lugt, M. A. Van Roon, M. A. Van der Valk, G. J. A. Offerhaus, A. J. M. Berns, and P. Borst. 1993. Homozygous disruption of the murine *mdr2* P-glycoprotein gene leads to a complete absence of phospholipid from bile and to liver disease. *Cell.* **75:** 451–462.
9. Coleman, R., and K. Rahman. 1992. Lipid flow in bile formation. *Biochim. Biophys. Acta.* **1125:** 113–133.
10. Small, D. M. 1970. The formation of gallstones. *Adv. Intern. Med.* **16:** 243–264.
11. Verkade, H. J., H. Wolters, A. Gerding, R. Havinga, V. Fidler, R. J. Vonk, and F. Kuipers. 1993. Mechanism of biliary lipid secretion in the rat: a role for bile acid-independent bile flow. *Hepatology.* **17:** 1074–1080.
12. Cohen, D. E., M. Angelico, and M. C. Carey. 1989. Quasielastic light scattering evidence for vesicular secretion of biliary lipids. *Am. J. Physiol.* **257:** G1–G8.
13. Cohen, D. E., L. S. Leighton, and M. C. Carey. 1992. Bile salt hydrophobicity controls vesicle secretion rates and transformations in native bile. *Am. J. Physiol.* **263:** G386–G395.
14. Ulloa, N., J. Garrido, and F. Nervi. 1987. Ultracentrifugal isolation of vesicular carriers of biliary cholesterol in native human and rat bile. *Hepatology.* **7:** 235–244.
15. Rigotti, A., L. Núñez, L. Amigo, L. Puglielli, J. Garrido, M. Santos, S. González, G. Mingrone, A. Greco, and F. Nervi. 1993. Biliary lipid secretion: immunolocalization and identification of a protein associated with lamellar cholesterol carriers in supersaturated rat and human bile. *J. Lipid Res.* **34:** 1883–1894.
16. Pattinson, N. R. 1985. Solubilisation of cholesterol in human bile. *FEBS Lett.* **181:** 339–342.
17. Bartles, J. R., L. T. Braiterman, and A. L. Hubbard. 1985. Endogenous and exogenous domain markers of the rat hepatocyte plasma membrane. *J. Cell Biol.* **100:** 1126–1138.
18. Renston, R. H., G. Zsigmond, R. A. Bernhoft, S. J. Burwen, and A. L. Jones. 1983. Vesicular transport of horseradish peroxidase during chronic bile duct obstruction in the rat. *Hepatology.* **3:** 673–680.
19. Puglielli, L., L. Amigo, M. Arrese, L. Nunez, A. Rigotti, J. Garrido, S. Gonzalez, G. Mingrone, A. V. Greco, L. Accatino, and F. Nervi. 1994. Protective role of biliary cholesterol and phospholipid lamellae against bile acid-induced cell damage. *Gastroenterology.* **107:** 244–254.
20. Sömjen, G. J., Y. Merikovsky, P. Lelkes, and T. Gilat. 1986. Cholesterol-phospholipid vesicles in human bile: an ultrastructural study. *Biochim. Biophys. Acta.* **879:** 14–21.
21. Sömjen, G. J., and T. Gilat. 1983. A non-micellar mode of cholesterol transport in human bile. *FEBS Lett.* **156:** 265–268.
22. Sömjen, G. J., and T. Gilat. 1985. Contribution of vesicular and micellar carriers to cholesterol transport in human bile. *J. Lipid Res.* **26:** 699–704.
23. Möckel, G-M., S. Gorti, R. K. Tandon, R. Tanaka, and M. C. Carey. 1995. Microscope laser light scattering spectroscopy of vesicles within canaliculi of rat hepatocyte couplets. *Am. J. Physiol.* **269:** G73–G84.
24. Armstrong, M. J., and M. C. Carey. 1982. The hydrophobic–hydrophilic balance of bile salts: inverse correlation between reverse-phase high performance liquid chromatographic mobilities and micellar cholesterol-solubilizing capacities. *J. Lipid Res.* **23:** 70–80.
25. Cohen, D. E., and M. R. Leonard. 1995. Immobilized artificial membrane chromatography: a rapid and accurate HPLC method for predicting bile salt–membrane interactions. *J. Lipid Res.* **36:** 2251–2260.
26. Sippel, C. J., M. Ananthanarayanan, and F. J. Suchy. 1990. Isolation and characterization of the canalicular membrane bile acid transport protein of rat liver. *Am. J. Physiol.* **258:** G728–G737.
27. Novak, D. A., C. J. Sippel, M. Ananthanarayanan, and F. J. Suchy. 1991. Postnatal expression of the canalicular bile acid transport system of rat liver. *Am. J. Physiol.* **260:** G743–G751.
28. Crawford, J. M., C. A. Berken, and J. L. Gollan. 1988. Role of the hepatocyte microtubular system in the excretion of bile salts and biliary lipid: implications for intracellular vesicular transport. *J. Lipid Res.* **29:** 144–156.
29. Crawford, J. M., D. C. J. Strahs, A. R. Crawford, and S. Barnes. 1994. The role of bile salt hydrophobicity in hepatic microtubule-dependent bile salt secretion. *J. Lipid Res.* **35:** 1738–1748.
30. Hasty, D. L., and E. D. Hay. 1978. Freeze-fracture studies of the developing cell surface. II. Particle-free membrane blisters on glutaraldehyde-fixed corneal fibroblasts are artefacts. *J. Cell Biol.* **78:** 756–768.
31. Smithwick, E. B. 1985. Cautions, common sense, and rationale for the electron microscopy laboratory. *J. Electron Microsc. Tech.* **2:** 193–200.
32. Wisse, E., A. De Wilde, and R. De Zanger. 1983. Perfusion fixation of human and rat liver tissue for light and electron microscopy: a review and assessment of existing methods with special emphasis on sinusoidal cells and microcirculation. *In* Science of Biological Specimen Preparation. A. M. F. O'Hare, editor. SEM Inc. Chicago, IL. 31–38.
33. Hagen, S. J., J. S. Trier, and R. Dambrauskas. 1994. Exposure of the rat small intestine to raw kidney beans results in reorganization of absorptive cell microvilli. *Gastroenterology.* **106:** 73–84.
34. Hirsch, J. G., and M. E. Fedorko. 1968. Ultrastructure of human leukocytes after simultaneous fixation with glu-

taraldehyde and osmium tetroxide and "postfixation" in uranyl acetate. *J. Cell Biol.* **38:** 615–627.
35. Wisse, E. 1970. An electron microscopic study of the fenestrated endothelial lining of rat liver sinusoids. *J. Ultrastruct. Res.* **31:** 125–150.
36. Jones, A. L., D. L. Schmucker, J. S. Mooney, R. K. Ockner, and R. D. Adler. 1979. Alterations in hepatic pericanalicular cytoplasm during enhanced bile secretory activity. *Lab. Invest.* **40:** 512–517.
37. Crawford, J. M., S. Barnes, R. C. Stearns, C. L. Hastings, and J. J. Godleski. 1994. Ultrastructural localization of a fluorinated bile salt in hepatocytes. *Lab. Invest.* **71:** 42–51.
38. Ottensmeyer, F. P. 1984. Electron spectroscopic imaging: parallel energy filtering and microanalysis in the fixed-beam electron microscope. *J. Ultrastruct. Res.* **88:** 121–134.
39. Livesey, S. A., and J. G. Linner. 1989. Cryofixation methods for electron microscopy. *In* Low Temperature Biotechnology: Emerging Applications and Engineering Contributions. Book No. G00459. J. J. McGrath and K. R. Diller, editors. The American Society of Mechanical Engineers. 159–174.
40. Buescher, E. S., S. A. Livesey, J. G. Linner, K. M. Skubitz, and S. M. McIlheran. 1990. Functional, physical, and ultrastructural localization of CD15 antigens to the human polymorphonuclear leukocyte secondary granule. *Anat. Rec.* **228:** 306–314.
41. Lo, W., A. Mills, and J. R. F. Kuck. 1994. Actin filament bundles are associated with fiber gap junctions in the primate lens. *Exp. Eye Res.* **58:** 189–196.
42. Delecolle, B., R. N. Wombim, and G. Marchoux. 1992. Optimisation de la technique de l'immunomarquage à l'or sur sections ultrafines réalisées à partir d'echantillons fixés à la glutaraldehyde et au tétroxyde d'osmium et inclus dans une époxy-résine. *Cell. Molec. Biol.* **38:** 495–511.
43. Drenckhahn, D., and R. Dermietzel. 1988. Organization of the actin filament cytoskeleton in the intestinal brush border: a quantitative and qualitative immunoelectron microscope study. *J. Cell Biol.* **107:** 1037–1048.
44. Turley, S. D., and J. M. Dietschy. 1978. Re-evaluation of the 3α-hydroxysteroid dehydrogenase assay for total bile acids in bile. *J. Lipid Res.* **19:** 924–928.
45. Zar, J. 1974. Biostatistical Analysis. Prentice-Hall, Inc. Englewood Cliffs, NJ.
46. Gurantz, D., and A. F. Hofmann. 1984. Influence of bile acid structure on bile flow and biliary lipid secretion in the hamster. *Am. J. Physiol.* **247:** G736–G748.
47. Layden, T. J., and J. L. Boyer. 1978. Influence of bile acids on bile canalicular membrane morphology and the lobular gradient in canalicular size. *Lab. Invest.* **39:** 110–119.
48. Vial, J. D., F. R. Simon, and A. M. Mackinnon. 1976. Effect of bile duct ligation on the ultrastructural morphology of hepatocytes. *Gastroenterology.* **70:** 85–92.
49. Hardison, W. G. M., R. G. Weiner, D. E. Hatoff, and K. Miyai. 1983. Similarities and differences between models of extrahepatic biliary obstruction and complete biliary retention without obstruction in the rat. *Hepatology.* **3:** 383–390.
50. Small, D. M. 1967. Phase equilibria and structure of dry and hydrated egg lecithin. *J. Lipid Res.* **8:** 551–559.
51. Barr, V. A., and A. L. Hubbard. 1993. Newly synthesized hepatocyte plasma membrane proteins are transported in transcytotic vesicles in the bile duct-ligated rat. *Gastroenterology.* **105:** 554–571.
52. Ruetz, S., and P. Gros. 1994. Phosphatidylcholine translocase: a physiological role for the mdr2 gene. Cell. 77: 1071–1081.
53. Baatsen, P. H. W. W. 1993. Empirically determined freezing time for quick-freezing with a liquid-nitrogen-cooled copper block. *J. Microsc.* **172:** 71–79.
54. Lowe, P. J., S. G. Barnwell, and R. Coleman. 1984. Rapid kinetic analysis of the bile-salt-dependent secretion of phospholipid, cholesterol and a plasma-membrane enzyme into bile. *Biochem. J.* **222:** 631–637.
55. Cohen, D. E., M. Angelico, and M. C. Carey. 1990. Structural alterations in lecithin-cholesterol vesicles following interactions with monomeric and micellar bile salts: physical–chemical basis for subselection of biliary lecithin species and aggregative states of biliary lipids during bile formation. *J. Lipid Res.* **31:** 55–70.
56. Lee, R. M. K. W., R. McKenzie, K. Kobayashi, R. E. Garfield, J. B. Forrest, and E. E. Daniel. 1982. Effects of glutaraldehyde fixative osmolarities on smooth muscle cell volume, and osmotic reactivity of the cells after fixation. *J. Microsc.* **125:** 77–88.
57. Klösgen, B., and W. Helfrich. 1993. Special features of phosphatidylcholine vesicles as seen in cryo-transmission electron microscopy. *Eur. Biophys. J.* **22:** 329–340.
58. Bloom, M., E. Evans, and O. G. Mouritsen. 1991. Physical properties of the fluid lipid-bilayer component of cell membranes: a perspective. *Q. Rev. Biochem.* **24:** 293–397.
59. Morgenstern, E. 1991. Aldehyde fixation causes membrane vesiculation during platelet exocytosis: a freeze-substitution study. *Scanning Microsc.* **5:** S109–S115.
60. Schubert, R., K. Beyer, H. Wolburg, and K. Schmidt. 1986. Structural changes in membranes of large unilamellar vesicles after binding of sodium cholate. *Biochemistry.* **25:** 5263–5269.
61. Landmann, L., P. J. Meier, and L. Bianchi. 1990. Bile duct ligation-induced redistribution of canalicular antigen in rat hepatocyte plasma membranes demonstrated by immunogold quantitation. *Histochemistry.* **94:** 373–379.
62. Berryman, M. A., W. R. Porter, R. D. Rodewald, and A. L. Hubbard. 1992. Effects of tannic acid on antigenicity and membrane contrast in ultrastructural immunocytochemistry. *J. Histochem. Cytochem.* **40:** 845–857.
63. Usuda, N., H. Ma, T. Hanai, S. Yokota, T. Hashimoto, and T. Nagata. 1990. Immunoelectron microscopy of tissues processed by rapid freezing and freeze-substitution fixation without chemical fixatives: application to catalase in rat liver hepatocytes. *J. Histochem. Cytochem.* **38:** 617–623.
64. Nanci, A., M. Mazariegos, and M. Fortin. 1992. The use of osmicated tissues for Lowicryl K4M embedding. *J. Histochem. Cytochem.* **40:** 869–874.
65. Lee, T., N. Araki, and Y. Takashima. 1993. Development of the bile canalicular system in rat liver: with special reference to bile canalicular actin filaments and Mg^{2+}, Ca^{2+}-ATPase activity. *Acta Histochem. Cytochem.* **26:** 337–348.
66. Thibault, N., M. Maurice, M. Maratrat, A. Cordier, G. Feldmann, and F. Ballet. 1993. Effect of tauroursodeoxycholate on actin filament alteration induced by cholestatic agents. A study in isolated rat hepatocyte couplets. *J. Hepatol.* **19:** 367–376.
67. Marzolo, M. P., A. Rigotti, and F. Nervi. 1990. Secretion of biliary lipids from the hepatocyte. *Hepatology.* **12 Suppl.:** 134S–142S.
68. Wheeler, H. O., and K. K. King. 1972. Biliary excretion of lecithin and cholesterol in the dog. *J. Clin. Invest.* **51:** 1337–1350.
69. Cabral, D. J., and D. M. Small. 1989. Physical chemistry of bile. *In* Handbook of Physiology, Section 6: The Gastrointestinal System. Vol. 3: Salivary, Gastric, Pancreatic, and

Hepatobiliary system. S. G. Schultz, J. G. Forte, and B. B. Rauner, editors. American Physiological Society, Bethesda, MD. 621–662.
70. Accatino, L., M. Pizarro, N. Solis, and C. S. Koenig. 1995. Association of canalicular membrane enzymes with bile acid micelles and lipid aggregates in human and rat bile. *Biochim. Biophys. Acta.* **1243:** 33–42.
71. Hardison, W. G. M., D. E. Hatoff, D. Miyai, and R. G. Weiner. 1981. Nature of the bile acid maximum secretory rate in the rat. *Am. J. Physiol.* **241:** G337–G343.
72. Barnwell, S. G., P. J. Lowe, and R. Coleman. 1984. The effects of colchicine on secretion into bile of bile salts, phospholipids, cholesterol and plasma membrane enzymes: bile salts are secreted unaccompanied by phospholipids and cholesterol. *Biochem. J.* **220:** 723–731.
73. Häussinger, D., N. Saha, C. Hallbrucker, F. Lang, and W. Gerok. 1993. Involvement of microtubules in the swelling-induced stimulation of transcellular taurocholate transport in perfused rat liver. *Biochem. J.* **291:** 355–360.
74. Boyer, J. L., and C. J. Soroka. 1995. Microtubule dependent targeting of transporters to the apical membrane determines the canalicular excretion of bile acids in hepatocyte couplets. *Gastroenterology.* **109:** 1600–1611.
75. Roman, I. D., A. Thewles, and R. Coleman. 1995. Fractionation of livers following diosgenin treatment to elevate biliary cholesterol. *Biochim. Biophys. Acta.* **1255:** 77–81.
76. Verkade, J. J., M. J. Wolbers, R. Havinga, D. R. A. Uges, R. J. Vonk, and F. Kuipers. 1990. The uncoupling of biliary lipid from bile acid secretion by organic anions in the rat. *Gastroenterology.* **99:** 1485–1492.
77. Curran, M. J., F. S. Cohen, D. E. Chandler, P. J. Munson, and J. Zimmerberg. 1993. Exocytotic fusion pores exhibit semi-stable states. *J. Membr. Biol.* **133:** 61–75.
78. Donovan, J. M., and M. C. Carey. 1990. Separation and quantitation of cholesterol "carriers" in bile. *Hepatology.* **12 Suppl:** 94S–105S.
79. Carey, M. C., and J. T. LaMont. 1992. Cholesterol gallstone formation. 1. Physical-chemistry of bile and biliary lipid secretion. *Prog. Liver Dis.* **10:** 139–163.
80. Weibel, E. R., W. Staubli, H. R. Gnagi, and F. A. Hess. 1969. Correlated morphometric and biochemical studies on the liver cell. I. Morphometric model, stereological methods, and normal morphometric data for rat liver. *J. Cell Biol.* **42:** 68–91.